MNRAS **000**, 1–17 (2015) Preprint October 27, 2015 Compiled using MNRAS LATEX style file v3.0

Origin and properties of dual and offset AGN in a cosmological simulation at z=2

Lisa K. Steinborn[1⋆], Klaus Dolag[1,2], Julia M. Comerford[3], Michaela Hirschmann[4], Rhea-Silvia Remus[1], Adelheid F. Teklu[1,5]

[1] *Universitäts-Sternwarte München, Scheinerstr.1, D-81679 München, Germany*
[2] *Max-Plank-Institut für Astrophysik, Karl-Schwarzschild Strasse 1, D-85740 Garching, Germany*
[3] *Department of Astrophysical and Planetary Sciences, University of Colorado, Boulder, CO 80309, USA*
[4] *UPMC-CNRS, UMR7095, Institut d'Astrophysique de Paris, Boulevard Arago, F-75014 Paris, France*
[5] *Excellence Cluster Universe, Boltzmannstr. 2, D-85748 Garching, Germany*

Received in original form 2015 October 27th

ABSTRACT

In the last few years, it became possible to observationally resolve galaxies with two distinct nuclei in their centre. For separations smaller than 10kpc, dual and offset active galactic nuclei (AGN) are distinguished: in dual AGN, both nuclei are active, whereas in offset AGN only one nucleus is active. To theoretically study the origin of such AGN pairs, we employ a cosmological, hydrodynamic simulation with a large volume of $(182\mathrm{Mpc})^3$ from the set of Magneticum Pathfinder Simulations. The simulation self-consistently produces 35 resolved black hole (BH) pairs at redshift $z = 2$, with a comoving distance smaller than 10kpc. 14 of them are offset AGN and nine are dual AGN, resulting in a fraction of $(1.2 \pm 0.3)\%$ AGN pairs with respect to the total number of AGN. In this paper, we discuss fundamental differences between the BH and galaxy properties of dual AGN, offset AGN and inactive BH pairs and investigate their different triggering mechanisms. We find that in dual AGN, the corresponding BH from the less massive progenitor galaxy always accretes with a higher Eddington ratio and that dual AGN have similar BH masses. In contrast, in offset AGN, the active BH is typically more massive than its non-active counterpart. Furthermore, dual AGN in general accrete more gas from the intergalactic medium than offset AGN and non-active BH pairs. This highlights that merger events, particularly minor mergers, do not necessarily lead to strong gas inflows and thus, do not always drive strong nuclear activity.

Key words: methods: numerical, galaxies: active, evolution, nuclei, interactions, quasars: supermassive black holes

1 INTRODUCTION

During the last few years, large-scale hydrodynamic cosmological simulations were established as one of the most powerful tools to make predictions for the evolution of the baryonic structures in the Universe. Thanks to the increasing power of modern supercomputers, the resolution in these simulations could be increased, helping to resolve the morphological structures of galaxies, even producing disk galaxies, which was a long-standing problem in the past (Vogelsberger et al. 2014, Schaye et al. 2015, Remus et al. 2015, Teklu et al. 2015). Since numerical and physical effects appear on scales, which were not resolved before, the implemented physical models and numerical schemes have to be refined. Much progress was made in the field of BH growth. The original implementation of Springel et al. (2005) contains only thermal, radiative AGN feedback, where the surrounding gaseous medium is heated with a constant efficiency. However, AGN feedback is known to work in two different regimes, so-called radio- and quasar-mode, or more intuitive, jet- and radiative mode, being dominated by jets and by radiation, respectively. In general, the two modes represent different phases of super-massive BH (SMBH) growth. As long as enough gas is driven towards the centre of a galaxy the BH accretes close to the Eddington accretion rate (radiative mode). Instead, as soon as the accretion rate decreases due to gas consumption or heating via feedback processes, some AGN form enormous jets, while the radia-

⋆ E-mail: steinborn@usm.lmu.de

tive power is much less efficient than before (jet-mode). To account for these different modes of AGN feedback, several authors (Sijacki et al. 2007, Rosas-Guevara et al. 2015, Vogelsberger et al. 2013, Sijacki et al. 2015, Steinborn et al. 2015) introduced more detailed sub-grid models for cosmological simulations. These simulations reproduce several observational constraints successfully, for example the M-σ relation and the $M_\bullet - M_*$ relation (e.g. Magorrian et al. 1998, Tremaine et al. 2002, Häring & Rix 2004, McConnell & Ma 2013, Kormendy & Ho 2013), the AGN luminosity function (e.g. Hopkins et al. 2007) and the BH mass function (e.g. Marconi et al. 2004, Shankar et al. 2004, Shankar et al. 2009, Shankar 2013).

However, while much progress was made in the field of galaxy merger simulations (e.g. Van Wassenhove et al. 2012, Blecha et al. 2013, Volonteri et al. 2015b, Capelo et al. 2015) and zoomed-in simulations (e.g. Bellovary et al. 2011), in most cosmological simulations, the BHs are artificially kept in the centres of the galaxies by pinning them to the gravitational potential minimum (Blecha et al. 2015, Springel et al. 2005), although dislocated BHs are indeed observed (e.g. Müller-Sanchez et al. 2015, Allen et al. 2015, Comerford et al. 2015, Comerford et al. 2012, McGurk et al. 2011, Barth et al. 2008). These dislocated BHs are thought to originate from galaxy merger events. When both progenitor galaxies host an SMBH, a close pair of SMBHs can form. At the stage, when these BHs are separated by a few kpc, they can be observed as dual or offset AGN, which are also called proto super-massive binary BHs in the literature (Hudson et al. 2006). In dual AGN, both BHs are observed as AGN, whereas in offset AGN only one BH is active. Note that the expression 'offset AGN' is also used in literature for single AGN which are offset from the galaxy centre. In these cases, the offsets are thought to be caused by recoiling BHs after BH mergers (e.g. Sijacki et al. 2011, Volonteri & Madau 2008, Blecha et al. 2015). In contrast to BH pairs, recoiling BHs are not self-consistently produced by cosmological simulations. Following Comerford et al. (2015), dual and offset AGN are BH pairs with a spatial separation of less than 10kpc. However, other maximum separations up to 100kpc exist in the literature (Koss et al. 2012).

In the local universe, offset AGN may be quite common (Comerford & Greene 2014, Comerford et al. 2009a, Comerford et al. 2013), while dual AGN might be more rare. In addition, they are still difficult to observe due to the small spatial separations. Although first evidence for the existence of dual AGN was already found by Owen et al. (1985), who observed two distinct radio jets in the radio source 3C 75 in Abell 400, only a few dual AGN have been confirmed so far. To confirm dual AGN observationally, both nuclei need to be spatially resolved (Komossa et al. 2003, Hudson et al. 2006, Bianchi et al. 2008, Koss et al. 2011, Koss et al. 2012, Mazzarella et al. 2012, Shields et al. 2012). One possibility to find dual AGN is to search for double-peaked narrow AGN emission lines. However, a double-peak alone can also be produced by the kinematics of the narrow line region of a single AGN (Müller-Sanchez et al. 2015) and hence this method can only be used to select hypothetical dual AGN candidates (e.g. Comerford et al. 2009b, Comerford et al. 2011, Barrows et al. 2013). Using this method, Fu et al. (2011b), Liu et al. (2013), Comerford et al. (2015) and Müller-Sanchez et al. (2015) recently found seven dual AGN systems, in which the existence of dual AGN could have been subsequently confirmed, by spatially resolving two distinct nuclei with separations less than 10kpc.

These detections indicate that galaxy mergers might trigger AGN activity, but since observations only capture "one moment in time", it is still unclear, whether the AGN are actually triggered by the gas inflow due to merger events or whether they have already been luminous before the merger event, i.e., whether their nuclear activity is driven by internal processes or due to their location in the large-scale cosmic web. Related to that, it is also a matter of vigorous debate, why in some BH pairs both BHs are active, in others only one of them or even none is active.

To investigate the origin of the differences between dual AGN, offset AGN and inactive BH pairs and to explore the underlying driving mechanisms for AGN activity during galaxy mergers, we employ a large-scale cosmological simulation at redshift $z = 2$ with both a large volume of $(182\mathrm{Mpc})^3$ and sufficiently high resolution to properly resolve the morphology of galaxies. In this simulation, we do not artificially keep BHs in the galaxy centre, providing a first attempt to study BH pairs in a fully cosmological context, as suggested by Volonteri et al. (2015a).

The paper is structured as follows. In Section 2, we briefly introduce our simulation and the BH model. We present our sample of BH pairs in Section 3 and discuss our results in Section 4. In Section 5, we compare our results to other theoretical studies and finally, we summarize our main results in Section 6.

2 THE SIMULATION

2.1 Set-up

For this study we use a simulation taken from the Magneticum Pathfinder Simulation set[1] (Dolag et al. in prep.), which is an ensemble of cosmological simulations including full hydrodynamics based on the TreePM-SPH code P-GADGET3 (Springel 2005). We assume a standard ΛCDM cosmology, where the Hubble parameter is $h = 0.704$ and the density parameters for matter, dark energy and baryons are $\Omega_\mathrm{m} = 0.272$, $\Omega_\Lambda = 0.728$ and $\Omega_\mathrm{b} = 0.0451$, respectively (WMAP7, Komatsu et al. 2011). The Magneticum Simulations contain sub-resolution models for star formation (Springel & Hernquist 2003), isotropic thermal conduction (Dolag et al. 2004) with an efficiency of $\kappa = 1/20$ of the classical *Spitzer* value (Arth et al. 2014), stellar evolution, metal enrichment and supernova feedback (Tornatore et al. 2003, Tornatore et al. 2007) as well as a cooling function which depends on the individual metal species following Wiersma et al. (2009). Furthermore, we use an updated viscosity treatment (Dolag et al. 2005, Beck et al. 2015) and Wendland kernels from Dehnen & Aly (2012), see Donnert et al. (2013) and Beck et al. (2015).

We use the same simulation set-up as described in Steinborn et al. (2015), but a higher resolution, with particle masses $M_\mathrm{dm} = 3.6 \cdot 10^7 M_\odot/h$ and $M_\mathrm{gas} = 7.3 \cdot 10^6 M_\odot/h$. The softening length is $1.4\mathrm{kpc}/h$ for dark matter and gas and $0.7\mathrm{kpc}/h$ for stars, allowing us to resolve BH pairs roughly

[1] magneticum.org

down to 2kpc, which is twice as large as the softening length of the stars (see Teklu et al. 2015 and Remus et al. in prep. 2015 for a detailed study of galaxy properties at this resolution level). To get a representative sample of BH pairs, we performed a large simulation with a volume of $(182\mathrm{Mpc})^3$ and an initial particle number of 7.2 billion particles down to redshift $z = 2$, where we find many BH pairs due to the rather high merger rate at that time.

2.2 Model for BH growth

The implementation of BH physics is based on Springel et al. (2005), in which BHs are treated as collision-less sink particles. In contrast to this original implementation, we use a more detailed description of AGN feedback and BH accretion according to Steinborn et al. (2015). In this model, we account for both radiation and mechanical outflows, which are implemented as thermal feedback. The radiative efficiency ϵ_r as well as the efficiency of mechanical outflows ϵ_o is variable and depends on the accretion rate onto the BH $\dot{M}_\bullet$ and on the BH mass $M_\bullet$, as induced by observations (Davis & Laor 2011, Chelouche 2013). We fix the coupling factor of the radiation to the surrounding medium to $\epsilon_\mathrm{f} = 0.03$. This value is chosen such that the simulation reproduces the normalization of the observed $M_\bullet$-M_* relation from McConnell & Ma (2013). Since this factor depends on the resolution, it is clearly lower than the value $\epsilon_\mathrm{f} = 0.2$ from Steinborn et al. (2015).

The accretion rate is limited to the Eddington accretion rate $\dot{M}_\mathrm{Edd}$ and furthermore, we distinguish between hot and cold gas accretion:

$$\dot{M}_\bullet = \min(\dot{M}_\mathrm{B,hot} + \dot{M}_\mathrm{B,cold}, \dot{M}_\mathrm{Edd}), \quad (1)$$

where both $\dot{M}_\mathrm{B,cold}$ and $\dot{M}_\mathrm{B,hot}$ are computed using the Bondi accretion rate (Hoyle & Lyttleton 1939, Bondi 1952, Bondi & Hoyle 1944). To account for turbulence following Gaspari et al. (2013), we multiply the cold gas accretion rate by the boost factor $\alpha = 100$ and the hot gas accretion rate by $\alpha = 10$. For further details regarding the sub-grid model for BH accretion and AGN feedback we refer the reader to Steinborn et al. (2015).

Furthermore, we do not perform any pinning of the BHs to the deepest potential in their surrounding as usually done, but let them evolve self-consistently. This prevents a too early merging of the BH sink particles and is only possible due to an improved numerically handling of the BH sink particles, which effectively avoids artificial drifting of such BH sink particles due to numerical inaccuracies as observed in the past (see Hirschmann et al. 2014 and Steinborn et al. 2015 for more details). Thereby, the BH sink particles evolve self-consistently during a merger event. Finally, we modified the conditions under which two BH sink particles will merge. Close pairs of BH sink particles will not be merged as long as they fulfill one of the following conditions: (i) the relative velocity of the BHs to each other is larger than $0.5 \cdot c_\mathrm{s}$, where c_s is the sound-speed of the surrounding gas; (ii) the distance is larger than five times the softening length and none of the two BHs is gravitationally bound to the other one. For too large separations between the BHs the second argument prevents a too early merging of the two BH sink particles. This approach still ignores any additional time the BHs need for the final merging, assuming that this timescale is still smaller than the dynamical time-steps of the cosmological simulation. Nevertheless, due to our novel approach in handling the BH sink particles, the final merging of the BHs in the simulations happens only in the very late state of the merger event, allowing us for the first time to study close BH pairs in cosmological simulations.

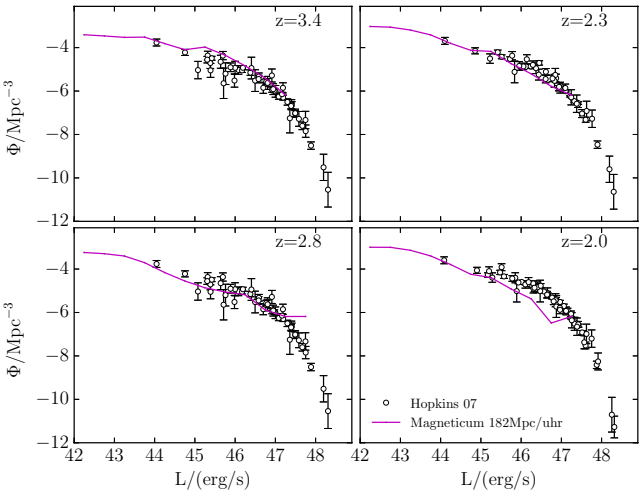

Figure 1. Bolometric AGN luminosity function of our simulation (solid magenta lines) at different redshifts in comparison to the observations (black circles with error bars) from Hopkins et al. (2007).

2.3 AGN luminosities

The bolometric AGN luminosities of our simulated BHs are calculated according to

$$L = \epsilon_\mathrm{r} \dot{M}_\bullet c^2. \quad (2)$$

Fig. 1 shows the bolometric AGN luminosity function at different redshifts. Our simulation (solid magenta lines) is successful in reproducing the observations from Hopkins et al. (2007) (black circles with error bars), particularly between $z = 3.4$ and $z = 2.3$. At lower redshifts, the simulation slightly underestimates the number density of AGN at the very bright end of the luminosity function. Note, however, that this can well be due to the inefficient size of the simulation volume. Our simulation at $z = 2$ contains only 19 AGN with $L_\mathrm{bol} > 10^{46}$, so a much larger volume would be needed to properly capture the bright end of the AGN luminosity function (see also Hirschmann et al. 2014). Nevertheless, the simulation volume is large enough to produce a statistically realistic population of AGN and therefore provides a good base to study dual and offset AGN for the first time in cosmological simulations.

3 SAMPLE OF BH PAIRS

Our simulation contains a total number of 14,903 BHs at $z = 2$ which are more massive than $10^7 M_\odot$. BHs below that mass have just been seeded and the system did not yet have time to evolve into a self-regulated state. We identify a sample of 34 BH pairs with a comoving distance smaller

than 10kpc at $z = 2$, where at least one BH is resolved in mass. This mass threshold corresponds roughly to our resolution limit for BHs, as shown in the BH mass function in Hirschmann et al. (2014). Throughout this paper, we define a BH as an AGN if it has a bolometric luminosity larger than 10^{43} erg/s. We distinguish between four different classes of BH pairs:

- dual AGN,
- offset AGN (both BHs are more massive than $10^7 M_\odot$),
- unresolved offset AGN (while the AGN is more massive than $10^7 M_\odot$, the second BH is below this resolution limit), and
- dual BHs without AGN.

Since in unresolved offset AGN, the non-active BH should actually be more massive, and since the luminosity depends on the BH mass, BH pairs in this class would be either classified as dual AGN or offset AGN, if the masses of both BHs were resolved.

Our chosen luminosity threshold is clearly arbitrary and leads to some overlap between the properties of the different classes of BH pairs. We refer to Section 5, in particular Fig. 14, where we show the contribution of the four different classes for different luminosity thresholds. However, we want to emphasize that a different definition does not change our results qualitatively.

Assuming that luminosity threshold, our sample of 34 BH pairs then splits up into:

- 9 dual AGN pairs (∼0.5% of all AGN),
- 6 offset AGN (∼0.3% of all AGN),
- 8 unresolved offset AGN (∼0.4% of all AGN) and
- 11 dual BHs without AGN.

Fig. 2 shows the fraction of dual and offset AGN with respect to the total amount of AGN for a given luminosity bin. The simulation predictions for $z = 2$ are shown by red diamonds, where the red error bars illustrate the corresponding $\sqrt{N}/N_{\rm tot}$ error. Note that our low number of AGN pairs leads to a rather large scattering. Since our simulation ran only down to $z = 2.0$, we cannot directly compare it with observations, which are only available for very low redshifts. Nevertheless, we include the best fit from Comerford & Greene (2014) for offset AGN candidates at $z < 0.21$ (black dotted line). Our simulated fraction of AGN/BH pairs at $z = 2.0$ covers the same range as the observed one at $z < 0.21$. Comerford & Greene (2014) found that the amount of candidate offset AGN increases with AGN luminosity at $z < 0.21$. Assuming that this correlation holds for higher redshifts, we agree with these results. This also confirms other observational results in the sense that the fraction of AGN triggered by galaxy mergers seems to increase with AGN luminosity (e.g. Treister et al. 2012).

Since our 182Mpc/uhr simulation contains 1864 AGN[2], the fraction of dual and offset AGN is ∼ 1.2% and the fraction of dual AGN varies between ∼ 0.48% and ∼ 0.91%, accounting for the fact that the unresolved offset AGN might actually be dual AGN. This agrees with the estimate of Rosario et al. (2011) at $z \sim 0.35$, where their results indicate

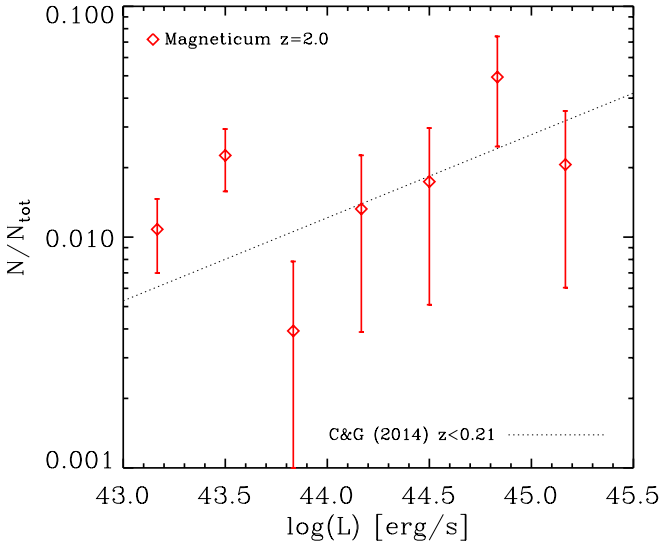

Figure 2. The red diamonds show the fraction of AGN in pairs with respect to the total number of AGN in bins of the bolometric luminosity, where N is the number of offset and dual AGN in bins of the bolometric luminosity and $N_{\rm tot}$ is the total number of AGN in the same luminosity range. The error bars show the corresponding $\sqrt{N}/N_{\rm tot}$ error. We also show the best fit for observed offset AGN candidates from Comerford & Greene (C&G, 2014) for redshifts $z < 0.21$ as black dotted line. Although their redshifts are much lower than $z = 2.0$, our fraction of AGN in BH pairs is similar.

that 0.3–0.65% of all AGN should be dual AGN systems. Our predicted fraction is, however, larger than the estimate from Fu et al. (2011a), who find that less than 0.3% of their SDSS sample at $0.03 < z < 0.56$ should be AGN in double systems.

In Tables 1 and 2, we summarize the most important properties of the simulated dual and offset AGN pairs, where d is the comoving distance of the BHs to each other and the indices 1 and 2 correspond to the more and less luminous AGN. We see no dependence of the luminosities on the distance between the BHs. We calculated the luminosities L_1 and L_2 of the two BHs as described in Steinborn et al. (2015). The Eddington ratios $f_{\rm Edd1}$ and $f_{\rm Edd2}$ are defined as $f_{\rm Edd} := L/L_{\rm Edd}$. [3]

Fig. 3 shows the cumulative fraction of dual and offset AGN for a given maximum separation $d_{\rm max}$ between the two BHs. The coloured areas indicate the contribution from the four different classes of BH pairs: dual AGN (red), offset AGN (blue), unresolved offset AGN (yellow) and BH pairs without AGN (green). Although our sample size is rather small, it is clearly visible that dual AGN dominate at small separations, whereas BH pairs without AGN are – in contrast to dual and offset AGN – more likely to be found at large distances. Furthermore, all resolved offset AGN have separations larger than 4kpc. This is also the case for the unresolved offset AGN, except for one example with an ex-

[2] Dual AGN pairs are counted as one AGN to be consistent with observations.

[3] Note that in our model this is not the same as $\dot{M}_\bullet/M_{\rm Edd}$ (Steinborn et al. 2015), since the total accretion rate splits up into luminosity and mechanical outflows.

ID	d [kpc]	$\log(L_1)$ [erg/s]	$\log(L_2)$ [erg/s]	$M_{\bullet 1}[M_\odot]$	$M_{\bullet 2}[M_\odot]$	$f_{\rm Edd1}$	$f_{\rm Edd2}$
1	9.68	43.58	43.57	$5.94 \cdot 10^7$	$4.42 \cdot 10^7$	$5.14 \cdot 10^{-3}$	$6.73 \cdot 10^{-3}$
2	8.78	43.20	43.06	$2.90 \cdot 10^7$	$4.16 \cdot 10^7$	$4.38 \cdot 10^{-3}$	$2.20 \cdot 10^{-3}$
3	2.40	43.20	43.17	$2.88 \cdot 10^7$	$1.84 \cdot 10^7$	$4.40 \cdot 10^{-3}$	$6.41 \cdot 10^{-2}$
4	2.67	44.77	44.76	$4.49 \cdot 10^7$	$3.62 \cdot 10^7$	$1.04 \cdot 10^{-1}$	$1.27 \cdot 10^{-1}$
5	8.91	45.32	43.49	$1.39 \cdot 10^8$	$2.04 \cdot 10^7$	$1.21 \cdot 10^{-1}$	$1.20 \cdot 10^{-2}$
6	3.50	43.42	43.33	$1.52 \cdot 10^8$	$1.19 \cdot 10^8$	$1.37 \cdot 10^{-3}$	$1.43 \cdot 10^{-3}$
7	8.25	44.53	43.35	$3.97 \cdot 10^8$	$1.59 \cdot 10^8$	$6.83 \cdot 10^{-3}$	$1.12 \cdot 10^{-3}$
8	7.11	44.46	44.06	$3.79 \cdot 10^7$	$5.10 \cdot 10^6$	$6.11 \cdot 10^{-2}$	$1.81 \cdot 10^{-1}$
9	7.17	44.72	43.20	$2.35 \cdot 10^7$	$8.98 \cdot 10^6$	$1.79 \cdot 10^{-1}$	$1.40 \cdot 10^{-2}$

Table 1. Properties of the dual AGN pairs in our simulation at $z = 2.0$. The indices 1 and 2 always correspond to the more and less luminous BH, respectively. The two dual AGN below the horizontal line contain one BH with $M_\bullet < 10^7 M_\odot$.

ID	d [kpc]	$\log(L_1)$ [erg/s]	$\log(L_2)$ [erg/s]	$M_{\bullet 1}[M_\odot]$	$M_{\bullet 2}[M_\odot]$	$f_{\rm Edd1}$	$f_{\rm Edd2}$
10	5.05	43.59	41.82	$1.57 \cdot 10^8$	$1.62 \cdot 10^7$	$1.97 \cdot 10^{-3}$	$3.26 \cdot 10^{-4}$
11	9.23	43.26	42.65	$6.94 \cdot 10^7$	$4.29 \cdot 10^7$	$2.09 \cdot 10^{-3}$	$8.37 \cdot 10^{-4}$
12	5.91	43.01	41.80	$2.72 \cdot 10^7$	$2.52 \cdot 10^7$	$3.00 \cdot 10^{-3}$	$1.99 \cdot 10^{-4}$
13	6.85	44.20	42.88	$5.14 \cdot 10^7$	$4.38 \cdot 10^7$	$2.44 \cdot 10^{-2}$	$1.37 \cdot 10^{-3}$
14	4.83	43.49	40.16	$5.71 \cdot 10^8$	$1.08 \cdot 10^8$	$4.30 \cdot 10^{-4}$	$1.73 \cdot 10^{-6}$
15	7.91	43.59	42.37	$1.49 \cdot 10^8$	$3.13 \cdot 10^7$	$2.08 \cdot 10^{-3}$	$5.88 \cdot 10^{-4}$
16	8.88	44.68	37.23	$3.52 \cdot 10^8$	$1.24 \cdot 10^6$	$1.07 \cdot 10^{-2}$	$1.10 \cdot 10^{-7}$
17	1.40	43.44	41.79	$1.04 \cdot 10^7$	$6.19 \cdot 10^6$	$2.10 \cdot 10^{-2}$	$7.89 \cdot 10^{-4}$
18	7.76	43.77	41.51	$4.57 \cdot 10^7$	$2.51 \cdot 10^6$	$1.02 \cdot 10^{-2}$	$1.03 \cdot 10^{-3}$
19	7.41	43.40	40.98	$1.35 \cdot 10^7$	$2.41 \cdot 10^6$	$1.48 \cdot 10^{-2}$	$3.12 \cdot 10^{-4}$
20	9.16	43.39	41.82	$4.59 \cdot 10^7$	$3.21 \cdot 10^6$	$4.23 \cdot 10^{-3}$	$1.65 \cdot 10^{-3}$
21	5.94	44.03	39.79	$1.04 \cdot 10^8$	$2.50 \cdot 10^6$	$8.20 \cdot 10^{-3}$	$1.97 \cdot 10^{-5}$
22	5.59	43.14	39.34	$2.92 \cdot 10^7$	$1.22 \cdot 10^6$	$3.74 \cdot 10^{-3}$	$1.42 \cdot 10^{-5}$
23	6.20	45.21	39.66	$1.36 \cdot 10^7$	$1.23 \cdot 10^6$	$9.45 \cdot 10^{-1}$	$2.98 \cdot 10^{-5}$

Table 2. Same as table 1 but for resolved (upper 6 lines) and unresolved (lower 8 lines) offset AGN.

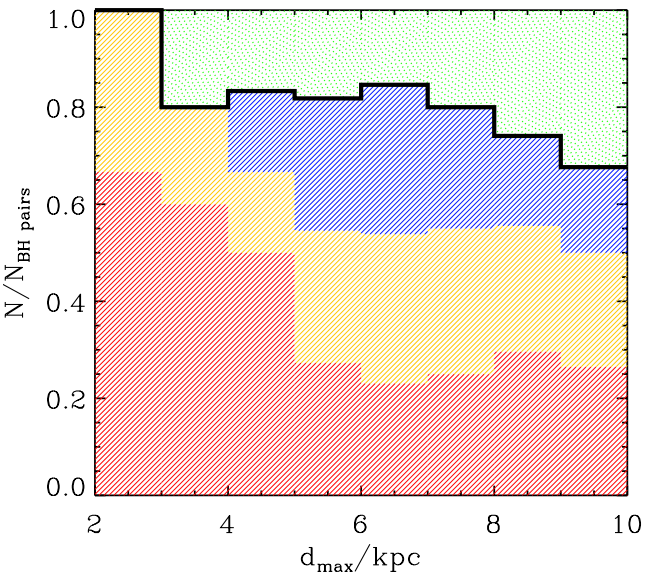

Figure 3. The black line shows the cumulative fraction of dual and offset AGN in bins of the maximum separation $d_{\rm max}$ between the two BHs. The coloured areas indicate the contribution from dual AGN (red), offset AGN (blue), unresolved offset AGN (yellow) and BH pairs without AGN (green).

tremely low separation. Note that, if the mass of the inactive BH was resolved, it could also be a dual AGN instead of an offset AGN. Overall, our simulation predictions are consistent with the observations from Comerford et al. (2015) indicating that the fraction of AGN increases with decreasing BH distances. This continues the trend which is observed for larger separations between 10kpc and 100kpc (Ellison et al. 2011, Koss et al. 2012).

In Fig. 4, we show visualizations[4] of a few examples of the three different classes of AGN/BH pairs. The images illustrate the baryonic component only. Gas and stars are colour-coded by the gas temperature and the stellar age, respectively (as indicated by the colour bars). The positions of all BH pairs are highlighted as coloured circles, where the colours red, blue, yellow and green represent dual AGN pairs, offset AGN, unresolved offset AGN and BH pairs without AGN, respectively. At first sight, there seems to be no obvious difference between the environment of the different types, which may be a consequence of overlaid structures due to the large volume. For three examples, we additionally show a smaller box of 10Mpc/h around the BH pair. We show larger illustrations of these regions in the three medium sized images at the middle top and middle bottom. The panel at the bottom demonstrates, for example, that

[4] performed with the free software Splotch, http://www.mpa-garching.mpg.de/~kdolag/Splotch from Dolag et al. (2008)

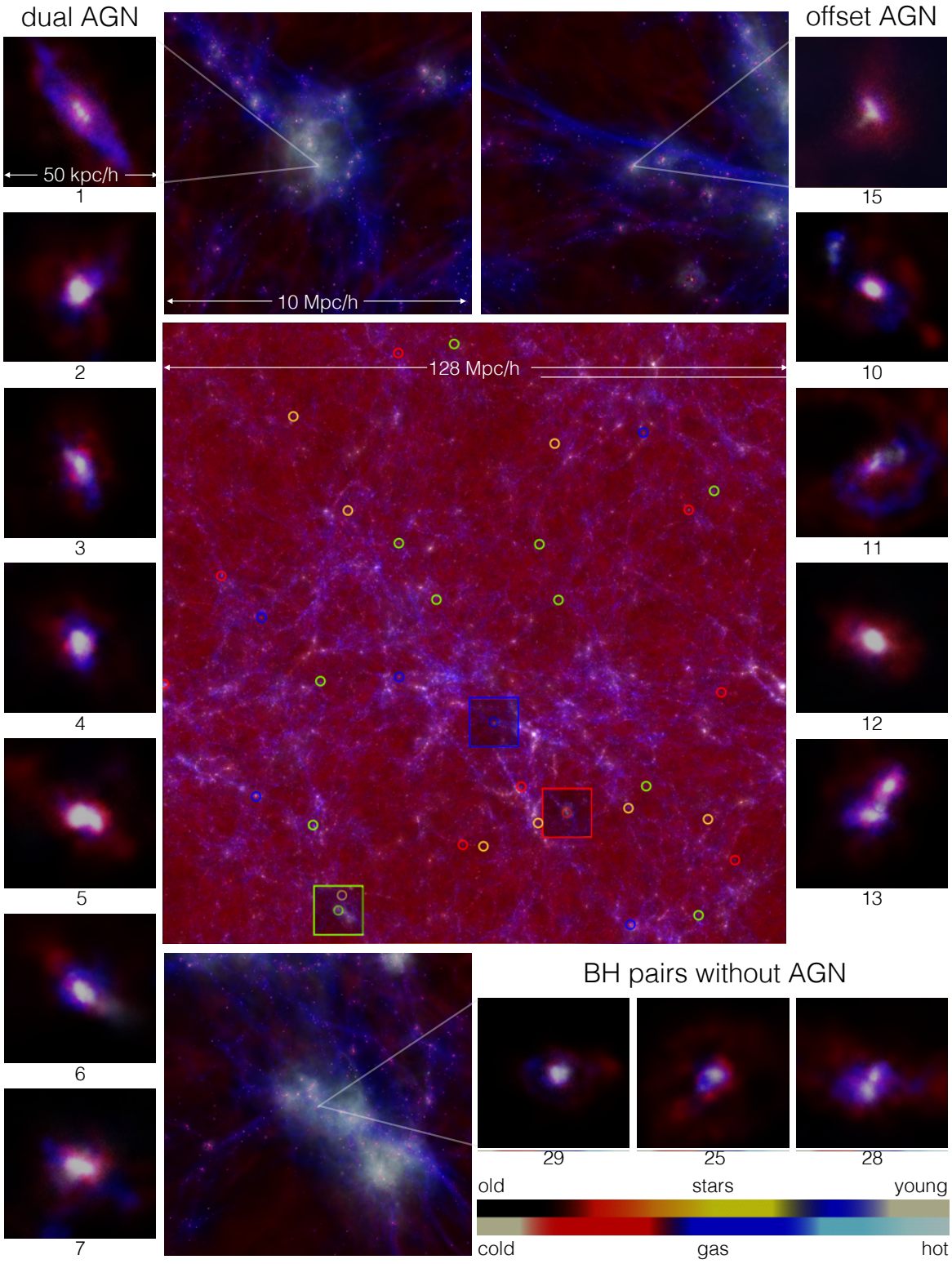

Figure 4. The large panel in the middle shows a visualization of our cosmological simulation. The red, blue and green circles mark the positions of all dual AGN pairs, offset AGN and BH pairs without AGN, respectively. Exemplarily, we show the large-scale environment, i.e. a box of 10 Mpc/h length around the host galaxy of one dual AGN pair, one offset AGN and one BH pair without AGN. The positions of these boxes are also marked in the large picture. We remark that the box is so large that structures are often not visible because they are overlaid by something else. Furthermore, we show a few examples of the host galaxies of the dual AGN (left images), offset AGN (right images) and BH pairs without AGN (images in the middle bottom), where we always show a box with a length of 70 kpc/h. The IDs of the BH pairs are the same as in Table 1 and 2 and the numbering continues to BH pairs without AGN (IDs 24-34). The colour bars are the same for all pictures, where the upper colour bar represents the age of the stars (from young to old) and the lower one the gas temperature (from cold to hot).

non-active BHs are not necessarily located in a gas poor environment. Overall, we can suspect that, in contrast to offset AGN and inactive BH pairs, dual AGN (left large image at the top) have a higher probability to be located in the centre of large-scale filaments, which can provide the gas supply for the galaxy. In Section 4.4 we will address this issue in more detail.

4 RESULTS

In this section, we investigate different properties of the BH pairs to understand the underlying mechanisms leading to the differences in their AGN activity.

4.1 BH and stellar masses

In the following figures, we illustrate dual AGN as red stars, offset AGN and their less luminous counterparts are represented by blue diamonds, unresolved offset AGN and their counterparts are illustrated by yellow diamonds and dual BHs without AGN are shown as green squares. The more luminous BH in a pair is always represented by a large symbol and the less luminous one by a smaller one. Fig. 5 shows the masses of the BHs in our sample versus the stellar mass of their host galaxies. The black solid line illustrates the best fit for the observations of McConnell & Ma (2013) at $z = 0$. Fig. 5 demonstrates that above $M_\bullet \sim 7 \cdot 10^7 M_\odot$, all BHs are either dual or offset AGN. For lower masses, active and non-active BHs cover the same mass range. By definition, a few inactive BHs are below the resolution limit of $M_\bullet = 10^7 M_\odot$ (black dotted line). These BHs would not necessarily be inactive, if they were properly resolved, at least those classified as "unresolved offset AGN". Since BHs are seeded at $M_* \sim 6 \cdot 10^9 M_\odot$, the stellar mass of their host galaxies already increased a lot, whereas the BH growth might be suppressed. This could explain why the unresolved counterparts of offset AGN (small yellow diamonds) have even lower BH masses than the BHs in pairs without AGN (green squares). We suspect that without this seeding and resolution effect, our simulation might contain more dual AGN.

In contrast to their less luminous counterparts, offset AGN are mostly more massive, although some of them have clearly lower masses than the BHs in dual AGN. As expected, almost all BHs lie below the observed relation from McConnell & Ma (2013), since the merger triggered star formation activity starts earlier than the fuelling of the BHs and the actual BH merger. This is in excellent agreement with the findings from Kormendy & Ho (2013).

Note that some BHs have host galaxies with stellar masses below the seeding threshold of $M_* \sim 6 \cdot 10^9 M_\odot$, very likely as a consequence of stellar stripping due to the ongoing merger.

4.2 Triggering versus suppressing accretion

Comerford et al. (2015) found that all dual AGN and dual AGN candidates in their sample have one interesting similarity: the BH in the less luminous galaxy always has the higher Eddington ratio. Interestingly, for dual AGN, we find the same behaviour in our simulation. This is demonstrated

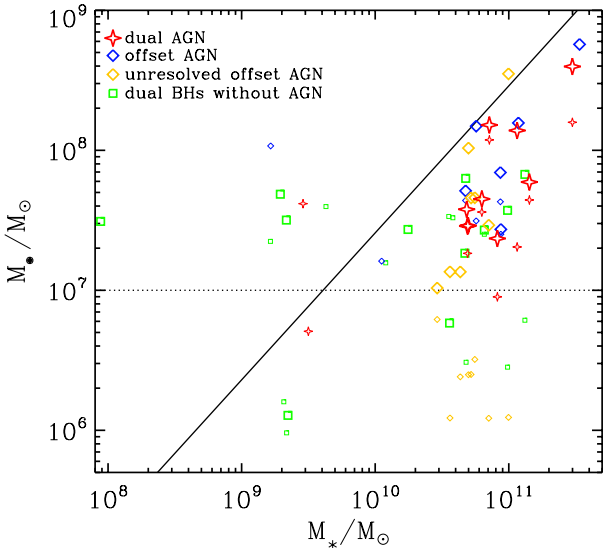

Figure 5. Relation between the BH mass and the stellar mass of the host galaxy for our sample of BH pairs. The different symbols illustrate the different classes of BH pairs, where large symbols correspond to the more luminous BHs in a pair and the small symbols to the less luminous ones. The black solid line shows the fit from McConnell & Ma (2013) and the black dotted line marks our resolution limit.

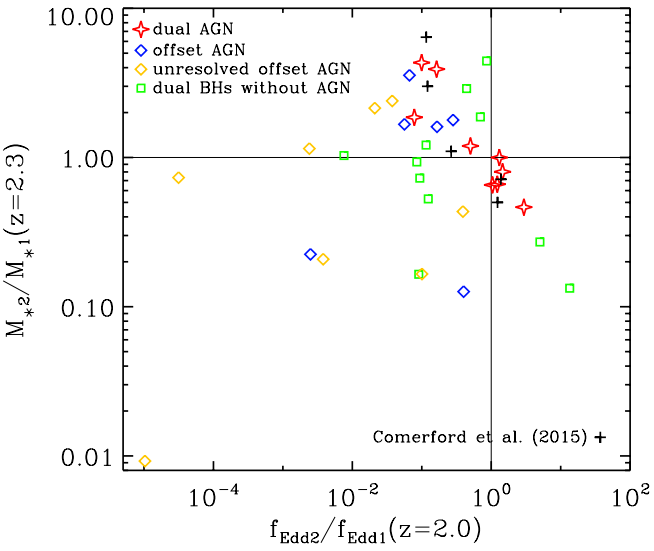

Figure 6. The ratio of the Eddington ratios compared to the stellar mass ratio. The indices 1 and 2 correspond to the more and less luminous BH, respectively. For all dual AGN the more luminous AGN originates from the less massive progenitor galaxy, whereas offset AGN always have a higher Eddington ratio than their less luminous counterpart. Our dual and offset AGN lie in the same range as observed ones (black crosses) from Comerford et al. (2015).

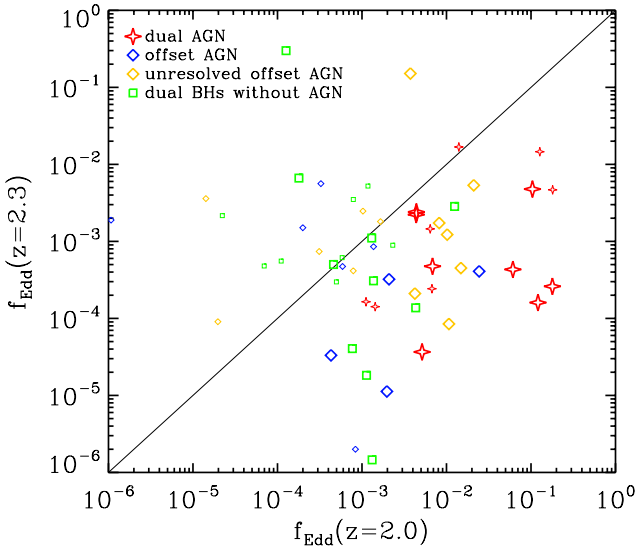

Figure 7. Comparison of the Eddington ratio at $z = 2.0$ and $z = 2.3$. For almost all dual AGN the Eddington ratio increases in this time interval. In pairs with only one AGN the Eddington ratio of the AGN increases, whereas it decreases for the less luminous BH. Dual BHs without AGN scatter in the range up to $f_{Edd} \approx 10^{-2}$. Note that some BH do not yet exist at $z = 2.3$ and hence, there are less than 60 data points.

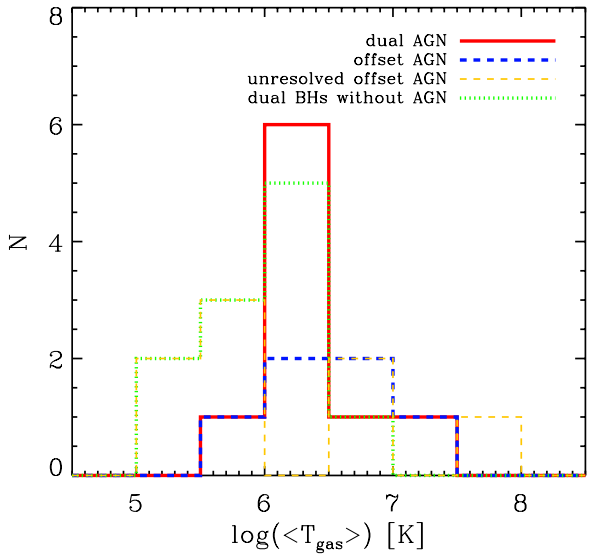

Figure 8. Distribution of the mean gas temperature inside the accretion radius. The figure shows only the gas temperatures around the less luminous BH, because we are interested in the mechanisms which suppress AGN activity in the less luminous counterparts of offset AGN (blue dashed histogram) and BH pairs without AGN (green dotted histogram) in contrast to dual AGN (red solid histogram).

in Fig. 6, showing the stellar mass ratio of the two progenitor galaxies at $z = 2.3$ versus the ratio of the corresponding Eddington ratios at $z = 2$. The indices 1 and 2 correspond to the more and less luminous BH, respectively. For dual AGN, the galaxy with the higher Eddington ratio has the lower stellar mass ratio and vice versa. Offset AGN, on the contrary, behave differently: as expected intuitively, the BH appearing as an AGN always has the higher Eddington ratio, irrespectively of the host galaxy mass. BH pairs without AGN activity can behave like both dual or offset AGN. Fig. 6 also shows that the simulation predictions cover the same range as the observed ones (black crosses).

To explore whether the AGN in our sample are actually triggered by the merger, we traced the BHs 0.5 Gyr back in time. Fig. 7 shows a comparison of the Eddington ratios at $z = 2.3$ and $z = 2.0$, where the symbols are the same as in Fig. 5. Non-active BHs scatter over the whole range, but mostly correspond to the jet-mode (or radio-mode), which is typically defined as $f_{Edd} < 5 \cdot 10^{-2}$. As shown in Steinborn et al. (2015), in this mode the gas reservoir in the vicinity of the inactive BHs is either heated or consumed, leading to rather low BH accretion rates and thus, low AGN luminosities.

For dual and offset AGN, the simulations predict one clear difference: for the majority of dual AGN, the Eddington ratio significantly increased between $z = 2.3$ and $z = 2.0$. Even if for both resolved and unresolved offset AGN, the Eddington ratio also increased, for their non-active counterparts (small blue and yellow diamonds), (except for one BH), it either hardly changes or it even decreases with time. We conclude that, in contrast to dual AGN, offset AGN might prevent their counterparts from accreting more gas. One possible explanation might be that offset AGN 'steal' gas from the second BH, since they are more massive and hence, attract the gas more strongly than the less massive BHs. We expect that for this scenario not only the mass difference of the BHs might play a role, but also the total mass difference of the two galaxies, which we will address in more detail in Section 4.3. Another explanation may be related to the effect of AGN feedback. Single BHs usually grow rapidly until AGN feedback and gas cooling are in equilibrium, where feedback leads to lower and gas cooling to higher accretion rates. When the equilibrium is reached, they grow along the M-σ relation (Churazov et al. 2005). In BH pairs, feedback from two BHs heats the same gas reservoir, and hence the heating may dominate compared to gas cooling, leading to low Eddington ratios. This could prevent the less massive BH from growing further, as it has 'starved' because of the feedback of the more massive BH, whereas the other BH is massive enough to appear as AGN also at low Eddington ratios.

To understand whether gravity or feedback dominates, we show in Fig. 8 the distribution of the mean gas temperature inside the accretion radius[5] of the less luminous BH. We are only interested in the less luminous BH, because whether AGN activity is suppressed in these BHs or not makes the difference between dual (red solid histogram) and offset AGN (blue dashed histogram), as we saw in Fig. 6 and Fig. 7. We find that most dual AGN have a surrounding gas temperature between 10^6K and $10^{6.5}$K. This indicates that AGN feedback already heats up the surrounding gas, but is still not strong enough to fully suppress the AGN activity. On the contrary, offset AGN (also the unresolved

[5] The accretion radius is set by the most distant gas particle used to calculate the Bondi accretion rate.

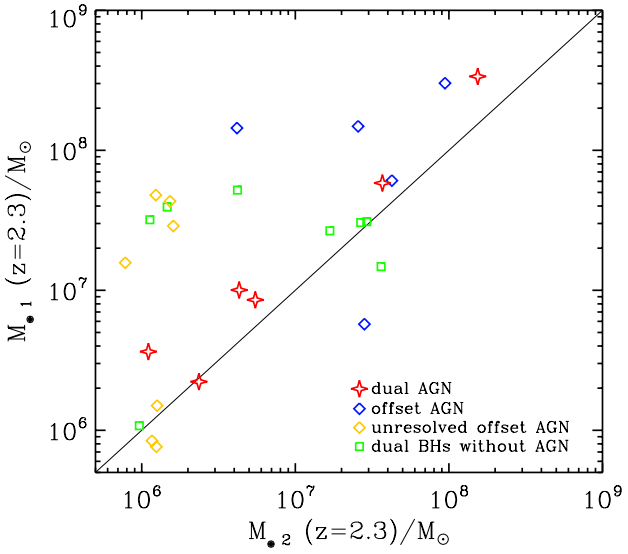

Figure 9. Comparison of the masses of the more ($M_{\bullet 1}$) and the less ($M_{\bullet 2}$) luminous BH around 0.5 Myr before (at $z = 2.3$) they were detected as dual BHs. For dual AGN the masses are similar, whereas for pairs with one or no AGN they can differ by more than one order of magnitude. BHs with masses lower than $5 \cdot 10^6 M_\odot$ are found in all three types of BH pairs. Again, there are less than 60 data points, because some BHs are not yet seeded at $z = 2.3$.

ones) do not peak in this range. The majority of the unresolved counterparts of offset AGN are surrounded by gas with a lower temperature and hence, AGN feedback is not important. We assume that gravity might play the most important role in these cases. However, there are also three resolved and three unresolved offset AGN which are surrounded by extremely hot gas ($> 10^{6.5}$K). There are also two dual AGN in this range. For the first of them the stellar masses of the progenitor galaxies are similar such that none of the BHs can dominate over the other one. In the second dual AGN pair the more luminous AGN has the less massive progenitor galaxy.

The green dotted histogram in Fig. 8 shows the temperature distribution around BH pairs without AGN. Five of these BHs are hosted by less massive young galaxies which contain a lot of cold gas but the BHs are simply too small to show AGN activity, although the distribution peaks in the same range as that of the dual AGN.

Finally, we would like to caution the reader that the gas temperature is not only affected by AGN feedback. However, in our cosmological simulation it is not possible to directly distinguish between different heating mechanisms, but since we consider only gas inside the accretion radius, the contribution of AGN feedback is probably large, especially for very high gas temperatures.

4.3 Merger mass ratio

To explicitly demonstrate the importance of the mass difference between the two merging BHs for the activity of BH pairs, we compare their masses in the snapshot before the merger, at $z = 2.3$ (see Fig. 9). It is evident that for dual AGN the BH masses are similar, whereas for pairs with one or no AGN, they can differ by more than one order of magnitude. This indicates that a large difference between the BH masses, and thus, also between the galaxy stellar masses, leads to a gas transfer from the smaller to the larger galaxy (e.g. review by Barnes & Hernquist 1992).

That offset AGN are a consequence of mergers with large mass differences, not only in the BH but also in the stellar mass, is supported by Fig. 17 and Fig. 18 in Appendix C, showing environmental dependencies of AGN pairs. Both dual and offset AGN pairs live in similar, rather high-density regions so that the large-scale environment is apparently not causing the different behaviour of BH pairs.

Fig. 10 illustrates the merger mass ratio of the BHs and the progenitor galaxies as a function of the gas mass of the galaxy hosting the BH pair at $z = 2.0$. Like in Fig. 6, M_{*1} and M_{*2} are the stellar mass of the galaxy with the more and less luminous BH at $z = 2.0$. For values below one, M_{*2}/M_{*1} equals the merger mass ratio, whereas for values larger than one it corresponds to the inverted merger mass ratio and the more luminous AGN originates from the less massive progenitor galaxy. We find that dual AGN preferably live in galaxies with a large gas content and a high stellar mass ratio. There are two exceptions with gas masses lower than $9 \cdot 10^{10} M_\odot$. In one of these galaxies the AGN have luminosities of $\log(L_1/(\mathrm{erg/s})) = 43.2$ and $\log(L_2/(\mathrm{erg/s})) = 43.2$, just above the threshold for our definition of AGN ($L > 10^{43}$erg/s). The other galaxy is located in the most massive cluster of the simulation, which has a total halo mass of $M_{\mathrm{halo}} = 1.3 \cdot 10^{14} M_\odot$ and is the only cluster with $M_{\mathrm{halo}} > 10^{14} M_\odot$ at $z = 2.0$. This might be a hint that AGN are triggered differently in a cluster environment. We suspect that in clusters not only the gas of the host galaxy but, also the gas reservoir of the whole cluster might feed the BH. Indeed, Krumpe et al. (2015) find that the mass of the dark matter halo is related to the BH mass. However, to take a closer look onto BH pairs in clusters, we would need lower redshifts and a larger sample of clusters, which is far beyond the scope of this paper.

Fig. 10 also illustrates that we can roughly distinguish between two different regimes for offset AGN: A large gas mass would, in principal, allow to feed both BHs, but, if one progenitor galaxy is much more massive than the other one, the gravitational potential dominates and hence, the BH residing in the more massive galaxy may use up the gas from the smaller one. Thus, offset AGN can have rather low stellar merger mass ratios, in contrast to dual AGN (see also Fig. 9). For lower gas masses, the merger mass ratio of dual AGN is still relatively large, i.e., all of them are major mergers, but as $M_{*2}/M*1 < 1$, this means that the more massive galaxy contains the more luminous BH. In contrast, offset AGN are hosted by the less massive galaxy, which again indicates that they are fed by the gas from the more massive galaxy during the merger, whereas the more massive BH already accreted much gas before the merger and eventually already heated up its surrounding gas.

But note that also other mechanisms than those described above might cause offset AGN, since some offset AGN reside in systems with intermediate gas masses and similar BH and stellar masses. In these cases, external forces, e.g., related to the environment, might play a role, which could distribute the gas such that one BH is surrounded by more gas than the other one.

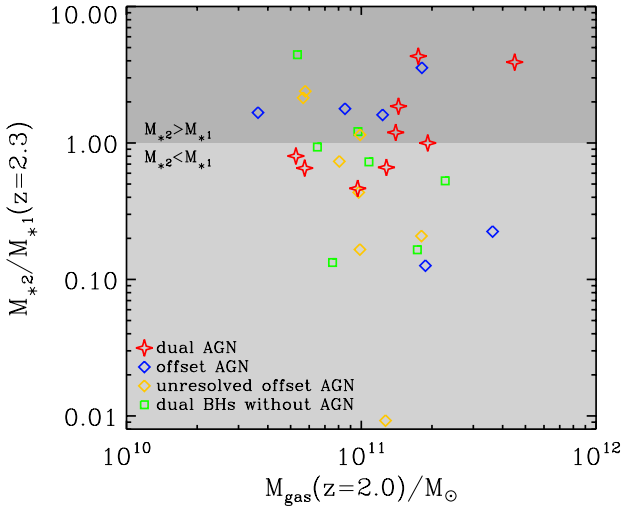

Figure 10. The stellar mass ratio of the progenitor galaxies at $z = 2.3$ in comparison with the gas mass of the galaxy hosting the BH pair at $z = 2.0$.

Interestingly, one offset AGN has also a relatively high gas mass, but a high mass ratio – the typical regime of most dual AGN. If we take a closer look at this BH pair, we find that the two BHs have a distance of 5.9 kpc with no overlap of the radii used for the calculation of the BH accretion rates. Furthermore, the more luminous BH (the AGN) was seeded during the last 0.5 Gyr and hence the luminosity peak might be an effect of our seeding model. Nevertheless, we find an interesting result when considering the progenitor galaxy of the AGN when looking at the galaxy morphology. As shown by Teklu et al. (2015), a good indicator for the galaxy morphology is the so-called b-value, which describes the position in the $M_* - j_*$-plane, where j_* is the specific angular momentum of the stars. The connection between morphology and the position on the $M_* - j_*$-plane was firstly noticed by Fall (1983) and was revisited by Romanowsky & Fall (2012), who proposed scaling relations for disks and elliptical galaxies, which would correspond to large and small b-values, respectively. Interestingly, the progenitor galaxy of the AGN has a very low b-value of -5.75, which is the lowest one in our sample and hence, the galaxy is very likely a compact elliptical galaxy. This comes along with a very low gas mass of $M_{\rm gas} = 2.1 \cdot 10^{10} M_\odot$. The stellar mass of this galaxy is also low with $M_* = 7.2 \cdot 10^9 M_\odot$ and the BH is not yet seeded at $z = 2.3$. The second progenitor galaxy has a larger stellar mass of $M_* = 2.6 \cdot 10^{10} M_\odot$, a larger gas mass of $M_{\rm gas} = 1.2 \cdot 10^{11} M_\odot$ and also a higher b-value of -4.57. We suspect that the gas from this galaxy feeds the BH from the smaller elliptical galaxy during the merger, whereas its own BH already accreted much gas in the past so that the surrounding gas has already been heated up by AGN feedback.

To summarize, the different outliers described in this subsection indicate that there exist no specific conditions for a BH pair to become a dual AGN pair or an offset AGN. Nonetheless, as expected, both the gas mass and the merger mass ratio are indeed crucial quantities for shaping different types of BH pairs.

4.4 Gas accretion history

In this section, we investigate the evolution of the gas content feeding the central BHs. Therefore, we trace the gas particles inside the accretion radius back in time and visualize the spatial distribution of these particles at $z = 2.3$, exemplary for two dual AGN pairs, two offset AGN and two BH pairs without AGN (see Fig. 11). Each panel shows a comoving volume of $(700\mathrm{kpc/h})^3$ at $z = 2.3$. The overall gas distribution is indicated by the contours, while the traced gas particles are indicated by the coloured circles. Blue and yellow circles mark gas from the host galaxy of the more and less luminous (luminosities at $z = 2.0$) BHs, respectively, whereas green circles are gas particles, which are associated to none of the two progenitor galaxies. The red cross and the red plus sign show the positions of the more and less luminous (again luminosities at $z = 2.0$) BHs, respectively.

The top panels show examples of dual AGN residing in gas filaments along which two galaxies merge. In these cases, gas from both progenitor galaxies, but also gas from the filament may feed the central BHs and thus, trigger nuclear activity, although the larger galaxy can contribute much more gas than the smaller one. For offset AGN, we show two fundamentally different cases. Almost all of the gas triggering AGN activity may originate from the smaller galaxy (see middle left panel). Alternatively, if the more massive galaxy has a large gas reservoir, the smaller BH may be simply not massive enough to "compete" with the massive one. The bottom panels show two examples for BH pairs without AGN. In both cases, gas from both the larger galaxy and the in-falling substructure as well as gas from outside the galaxies can contribute to the BH accretion rate. However, no matter, how large or small the overall gas reservoir around the BH is, the gas in these inactive BH pairs is typically spread over a larger area, i.e., the gas density is lower. This, together with the typically low BH masses, can explain the rather low BH accretion rates, since – according to the Bondi formalism – BH accretion rates scale with the gas density and the BH mass.

To quantify how strongly dual AGN might be triggered by gas filaments, we divide the traced gas particles into the three groups mentioned before: gas which was in progenitor galaxy 1, progenitor galaxy 2 or in none of them at $z = 2.3$. In the latter case, the gas was probably accreted by the galaxies between $z = 2.3$ and $z = 2.0$ either through gas filaments, the infall of gas clumps or additional minor mergers. Fig. 12 illustrates the distribution of the gas masses belonging to one of these three groups with respect to the total mass of all gas particles which contribute to the BH accretion. We show these distributions for dual AGN (red solid histogram), offset AGN (blue dashed histogram), unresolved offset AGN (yellow dashed histogram) and BH pairs without AGN (green dotted histogram), where we consider only the more luminous BH in a pair. The small vertical lines in the top indicate the mean values of each distribution. For dual AGN the contribution of gas, which was never residing in any of the two progenitor galaxies, is clearly enhanced compared to offset AGN and inactive BH pairs (see lowest panel of Fig. 12). This indicates that dual AGN indeed ac-

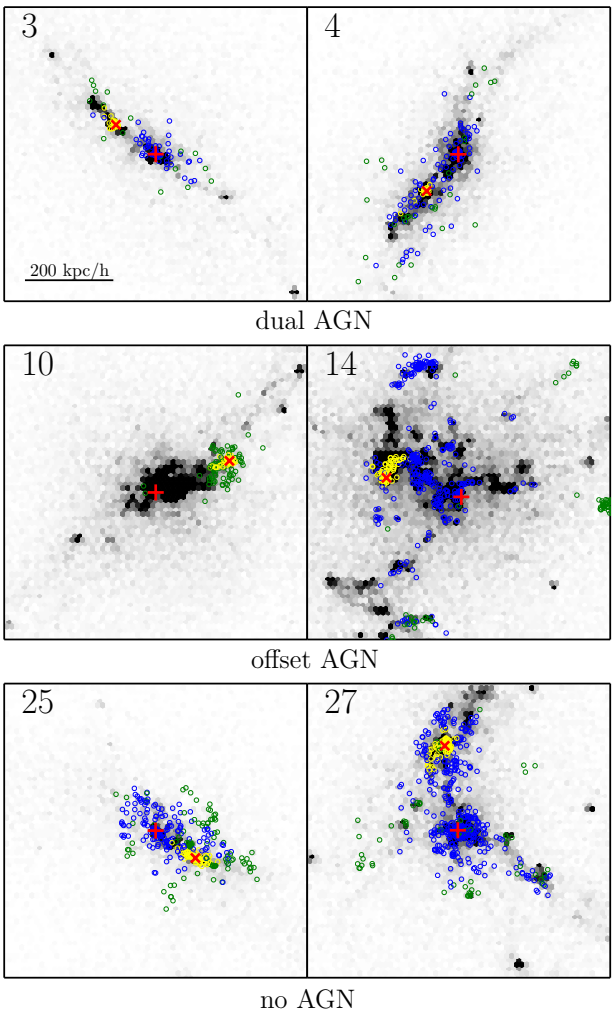

Figure 11. The figure shows the progenitor galaxies of two dual AGN pairs, two offset AGN and two BH pairs without AGN at $z = 2.3$, where the IDs are the same as in Table 1, Table 2 and Fig. 4. The grey shades visualize the overall gas distribution and the coloured circles show where the gas which is accounted for the estimation of the BH accretion rate comes from. Blue and yellow circles indicate gas from the progenitor galaxy of the more and less luminous BH, respectively, whereas green circles represent gas which was associated to none of the two galaxies. In every panel, the red plus sign marks the more luminous BH of the pair and the red 'x' sign the less luminous one.

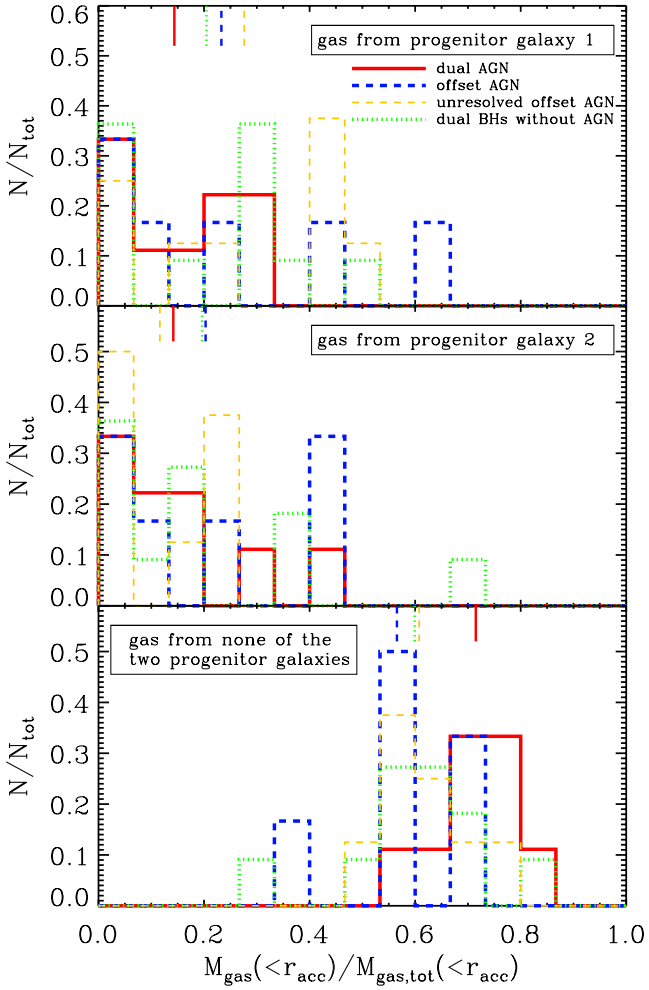

Figure 12. For this figure we traced back all gas particles inside the accretion radius at $z = 2.0$ and checked whether they have been in galaxy 1 (progenitor galaxy of the more luminous BH), galaxy 2 (progenitor galaxy of the less luminous BH) or in none of them at $z = 2.3$. The upper panel shows the gas mass from galaxy 1, the middle panel the gas mass from galaxy 2 and the bottom panel shows the gas mass which was hosted by neither of the two progenitor galaxies with respect to the total mass of the traced gas, respectively. The small vertical lines at the top indicate the mean values of each distribution.

crete more gas from filaments than the other, less active BH pairs.

In Fig. 13, we compare the contribution of the two galaxies to the calculation of the BH accretion with each other. Like in Fig. 12, it shows that for dual AGN in general less internal gas from the galaxies contributes to the BH accretion than for offset AGN. In most cases, this gas originates from both progenitor galaxies. In contrast, for the offset AGN mostly one of the two progenitor galaxies contributes much more gas to the BH accretion than the other one. This can be the progenitor galaxy of either the less luminous BH or the more luminous one. In the specific case of unresolved offset AGN, the progenitor galaxy of the more luminous BH is in most cases the main contributor.

5 COMPARISON WITH OTHER THEORETICAL STUDIES

In this section we will compare our results with other theoretical studies, i.e. Yu et al. (2011), Van Wassenhove et al. (2012) and Blecha et al. (2013), which use either phenomenological models or isolated merger simulations. Yu et al. (2011), for example, construct a phenomenological model for AGN pairs, and find that the fraction of dual AGN with respect to the total amount of AGN decreases significantly

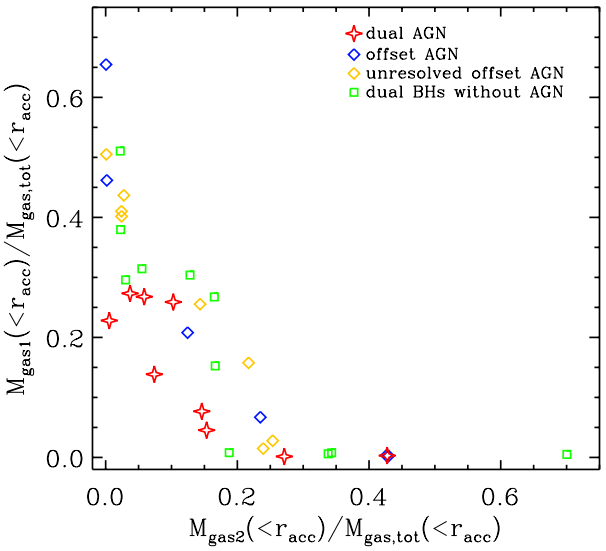

Figure 13. Comparison of the fraction of gas mass with respect to the total gas mass inside the accretion radius at $z = 2.0$ which comes from galaxy 1 and galaxy 2.

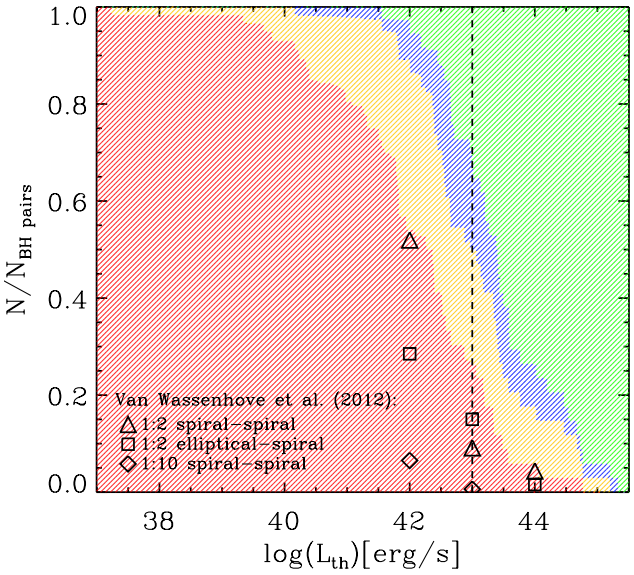

Figure 14. The coloured areas indicate the fraction of simulated dual AGN (red), offset AGN (blue), unresolved offset AGN (yellow) and BH pairs without AGN (green) with respect to the total number of BH pairs, if we choose different luminosity thresholds $L_{\rm th}$ for our definition of AGN. The black dashed line marks the threshold we choose for the analysis in this paper, i.e 10^{43}erg/s. The black symbols show the results from Van Wassenhove et al. (2012) for separations $d > 1$kpc with respect to the total amount of dual AGN and offset AGN only.

with redshift up to $z = 0.5$. In the range $0.5 < z < 1.2$, their models do not predict any significant change in the dual AGN fraction. Assuming that the frequency of dual AGN will also not increase significantly for higher redshifts up to $z = 2$, this is consistent with the Magneticum Simulations, which predict a clearly higher dual AGN fraction at $0.01 \leqslant z \leqslant 0.21$ than at $z = 2$ (Table 3 in the Appendix). The luminosity threshold from Yu et al. (2011), above which a BH is defined as an AGN, is $L_{[\rm OIII]} > 10^{7.5} L_{\odot}$, which roughly corresponds to $L_{\rm bol} > 10^{44.6}$erg/s assuming $L_{\rm bol}/L_{[\rm OIII]} \approx 3500$ (Heckman et al. 2004). Above this threshold they predict a dual AGN fraction of about 0.02%-0.06%. Our sample contains only one dual AGN which fulfills this condition corresponding to $\sim 0.05\%$, being in agreement with Yu et al. (2011). But we caution the reader since this value is based on only one dual AGN pair.

Van Wassenhove et al. (2012) performed three high resolution simulations of isolated galaxy mergers: (i) a 1:2 merger between two spiral galaxies, (ii) a 1:2 merger between an elliptical galaxy and a spiral galaxy and (iii) a 1:10 merger between two spiral galaxies. Their simulations are very good comparable to our results, because the two major mergers occur roughly around $z = 2$, while the minor merger occurs around 1 Gyr later. In agreement with our results, Van Wassenhove et al. (2012) find that the gas content and the merger mass ratio play an important role in triggering dual AGN activity. In their simulations, the fraction of dual AGN activity also increases with decreasing separation between the two BHs, which is consistent with our analysis (see Fig. 3).

In addition, Van Wassenhove et al. (2012) provide estimates for the dual AGN fraction with respect to the total number of dual and offset AGN for different luminosity thresholds. In Fig. 14, we show the contribution of the different types of our simulated BH pairs with respect to the total number of BH pairs, depending on the luminosity threshold $L_{\rm th}$, where the shaded areas illustrate the contribution of dual AGN (red), offset AGN (blue), unresolved offset AGN (yellow), and BH pairs without AGN (green). Our choice for the analysis in this work, i.e., $L_{\rm th} = 10^{43}$erg/s, is marked by the black dashed line. At that threshold, the contribution of the different types of BH pairs is similar. The different black symbols show the results of the three simulations from Van Wassenhove et al. (2012) for separations larger than 1kpc (by 1kpc higher resolution than ours). Furthermore, they do not have an upper limit for the BH separations, which should mainly affect the values at $L_{\rm th} = 10^{42}$erg/s, since they find that most AGN activity occurs at small separations, in particular above $L_{\rm th} = 10^{43}$erg/s. Nevertheless, we see a similar increase of the dual AGN fraction with decreasing luminosity threshold like for the 1:2 spiral-spiral merger from Van Wassenhove et al. (2012). In contrast to the major mergers, the number of BH pairs in minor mergers is smaller than our prediction and regarding the elliptical-spiral merger, the number of BH pairs is also smaller – except for $L_{\rm th} = 10^{43}$erg/s – than our estimate. We suspect that their estimates are in general lower than our predictions, because their spiral galaxies have a much lower gas fraction of $f_{\rm g} = 0.3$ than spiral galaxies in the Magneticum Simulations, where $f_{\rm g} \sim 0.6 - 0.8$ (Teklu et al. 2015). We conclude that dual AGN activity is indeed mainly triggered by gas-rich major mergers. Furthermore, we want to emphasize that we are in very good agreement with the results from Van Wassenhove et al. (2012) at $L_{\rm th} = 10^{45}$erg/s, where the effect of the maximum separation should not affect our results.

Finally, our results agree with those of Blecha et al.

(2013), who present hydrodynamic simulations of major mergers with different merger mass ratios and gas fractions. They also find that the dual AGN activity increases with both the merger mass ratio and the gas fraction, although the effect of the mass ratio is not entirely clear, probably due to the fact that they only consider major mergers. Furthermore, like Van Wassenhove et al. (2012), they find that the AGN activity is larger in the late phase of a merger, i.e. when the separations between the two BHs are small, which is also in agreement with our results.

6 CONCLUSION

In this study, we explore the properties and the origin of dual and offset AGN, taking advantage of a cosmological simulation covering $(182\mathrm{Mpc})^3$, taken from the set of Magneticum Pathfinder Simulations. The simulation includes an improved treatment of super-massive BHs and ran down to redshift $z = 2$. It predicts an evolution of the AGN luminosity function which is consistent with observations. The novel treatment of the black holes in the simulation offers a unique testbed to study the properties and evolution of BH pairs. At $z = 2$, the simulation contains 34 BH pairs with a comoving separation smaller than 10kpc. Nine of them are pairs of dual AGN, 6 are offset AGN and 8 are unresolved offset AGN, where the mass of the smaller counterpart is not resolved. However, the remaining 11 BH pairs show no actual AGN activity. As in the simulation all BH pairs originate from galaxy mergers, this implies that merger activity by itself is not always sufficient to trigger AGN activity. To investigate the mechanisms which trigger the AGN activity in detail, we traced the BHs, their progenitor galaxies and the gas which contributes to the calculation of the accretion rate back in time. Our main results are the following:

- We find that the merger mass ratio, the gas mass and the gas accretion history are important factors in triggering dual AGN activity.
- Dual AGN activity dominates for small spatial separations between the two BHs, whereas inactive BH pairs tend to have larger separations.
- Almost all BHs in pairs lie below the observed $M_\bullet$-M_* relation. Whilst the most massive BHs appear typically as AGN, less massive ones can be both, either active or non-active.
- In dual AGN pairs, the less massive progenitor galaxy always hosts the BH which lateron has the higher Eddington ratio.
- Dual AGN have similar BH masses and grow together, i.e., the Eddington ratio of both BHs in a pair increases during the merger.
- At $z = 2.0$, the gas which triggers dual and offset AGN consists mainly of freshly accreted gas, which encounters the progenitor galaxies during or right before the merger, probably through gas filaments or through accretion of smaller substructures. The contribution of this accretion to the BH accretion is on average clearly larger for dual AGN than for BH pairs with only one or no AGN.
- In most cases, one of the two progenitor galaxies contributes much more gas to the BH accretion than the other galaxy, especially for offset AGN. This can be either the progenitor galaxy of the more luminous or the less luminous BH.
- Offset AGN can exist in galaxies with relatively low gas masses, if the BH masses are so small that the gas reservoir is still large enough that at least one BH can accrete with a high Eddington ratio, i.e., in the radiatively efficient regime.
- Offset AGN can also be the consequence of a merger of a larger with a smaller galaxy, where the large BH accretes and heats up so much gas that it either uses up or evaporates the cold gas reservoir of the smaller BH.
- The same effect can be seen in BH pairs without AGN, with the difference that there is even for the more massive BH too little gas to accrete enough for being classified as an AGN.

This study is based on a state-of-the-art large-scale cosmological simulation for which for the first time not only the resolution is high enough to resolve galaxies, but also the volume is large enough to capture the generally rare events of dual AGN. With our sample of BH pairs, we can explain fundamental differences between dual AGN, offset AGN and inactive BH pairs. However, due to the limited computational power, we can only study the triggering mechanisms down to $z = 2.0$, where galaxy properties like the gas fraction are significantly different from observed dual and offset AGN at low redshifts. We expect that this does not qualitatively influence our results regarding the differences between dual and offset AGN, but with decreasing redshift, quantitative results are very likely to change. We expect, for example, that the contribution of smooth gas accretion might be less important for driving nuclear activity at lower redshifts. Since we find such a process to be essential for producing dual AGN, we may speculate that in the local Universe, a smaller amount of dual AGN may exist with respect to that of offset AGN.

In future work, we plan to extend this study, by investigating AGN trigger mechanisms and the relative role of internal and external processes, in global BH populations, and not only for BH pairs. This may shed further light on the still heavily debated question to what extent merger events are responsible (and needed) for driving nuclear activity.

ACKNOWLEDGMENTS

We are especially grateful for the support by M. Petkova through the Computational Center for Particle and Astrophysics (C2PAP). Computations have been performed at the 'Leibniz-Rechenzentrum' with CPU time assigned to the Project 'pr86re'. This research was supported by the DFG Cluster of Excellence 'Origin and structure of the universe' and the SFB-Tansregio TR33 'The Dark Universe'. MH acknowledges financial support from the European Research Council via an Advanced Grant under grant agreement no. 321323 NEOGAL.

References

Allen J. T., et al., 2015, MNRAS, 451, 2780
Arth A., Dolag K., Beck A. M., Petkova M., Lesch H., 2014, preprint, (arXiv:1412.6533)

Baldry I. K., Balogh M. L., Bower R. G., Glazebrook K., Nichol R. C., Bamford S. P., Budavari T., 2006, MNRAS, 373, 469
Barnes J. E., Hernquist L., 1992, ARA&A, 30, 705
Barrows R. S., Sandberg Lacy C. H., Kennefick J., Comerford J. M., Kennefick D., Berrier J. C., 2013, ApJ, 769, 95
Barth A. J., Bentz M. C., Greene J. E., Ho L. C., 2008, ApJ, 683, L119
Beck A. M., et al., 2015, preprint, (arXiv:1502.07358)
Bellovary J., Volonteri M., Governato F., Shen S., Quinn T., Wadsley J., 2011, ApJ, 742, 13
Bianchi S., Chiaberge M., Piconcelli E., Guainazzi M., Matt G., 2008, MNRAS, 386, 105
Blecha L., Loeb A., Narayan R., 2013, MNRAS, 429, 2594
Blecha L., et al., 2015, preprint, (arXiv:1508.01524)
Bondi H., 1952, MNRAS, 112, 195
Bondi H., Hoyle F., 1944, MNRAS, 104, 273
Capelo P. R., Volonteri M., Dotti M., Bellovary J. M., Mayer L., Governato F., 2015, MNRAS, 447, 2123
Chelouche D., 2013, ApJ, 772, 9
Churazov E., Sazonov S., Sunyaev R., Forman W., Jones C., Böhringer H., 2005, MNRAS, 363, L91
Comerford J. M., Greene J. E., 2014, ApJ, 789, 112
Comerford J. M., et al., 2009a, ApJ, 698, 956
Comerford J. M., Griffith R. L., Gerke B. F., Cooper M. C., Newman J. A., Davis M., Stern D., 2009b, ApJ, 702, L82
Comerford J. M., Pooley D., Gerke B. F., Madejski G. M., 2011, ApJ, 737, L19
Comerford J. M., Gerke B. F., Stern D., Cooper M. C., Weiner B. J., Newman J. A., Madsen K., Barrows R. S., 2012, ApJ, 753, 42
Comerford J. M., Schluns K., Greene J. E., Cool R. J., 2013, ApJ, 777, 64
Comerford J. M., Pooley D., Barrows R. S., Greene J. E., Zakamska N. L., Madejski G. M., Cooper M. C., 2015, ApJ, 806, 219
Davis S. W., Laor A., 2011, ApJ, 728, 98
Dehnen W., Aly H., 2012, MNRAS, 425, 1068
Dolag K., Jubelgas M., Springel V., Borgani S., Rasia E., 2004, ApJ, 606, L97
Dolag K., Vazza F., Brunetti G., Tormen G., 2005, MNRAS, 364, 753
Dolag K., Reinecke M., Gheller C., Imboden S., 2008, New Journal of Physics, 10, 125006
Donnert J., Dolag K., Brunetti G., Cassano R., 2013, MNRAS, 429, 3564
Ellison S. L., Patton D. R., Mendel J. T., Scudder J. M., 2011, MNRAS, 418, 2043
Fall S. M., 1983, in Athanassoula E., ed., IAU Symposium Vol. 100, Internal Kinematics and Dynamics of Galaxies. pp 391–398
Fu H., Myers A. D., Djorgovski S. G., Yan L., 2011a, ApJ, 733, 103
Fu H., et al., 2011b, ApJ, 740, L44
Gaspari M., Ruszkowski M., Oh S. P., 2013, MNRAS, 432, 3401
Haas M. R., Schaye J., Jeeson-Daniel A., 2012, MNRAS, 419, 2133
Häring N., Rix H.-W., 2004, ApJ, 604, L89
Heckman T. M., Kauffmann G., Brinchmann J., Charlot S., Tremonti C., White S. D. M., 2004, ApJ, 613, 109
Hirschmann M., Dolag K., Saro A., Bachmann L., Borgani S., Burkert A., 2014, MNRAS, 442, 2304
Hopkins P. F., Richards G. T., Hernquist L., 2007, ApJ, 654, 731
Hoyle F., Lyttleton R. A., 1939, Proceedings of the Cambridge Philosophical Society, 35, 405
Hudson D. S., Reiprich T. H., Clarke T. E., Sarazin C. L., 2006, A&A, 453, 433
Komatsu E., et al., 2011, ApJS, 192, 18
Komossa S., Burwitz V., Hasinger G., Predehl P., Kaastra J. S., Ikebe Y., 2003, ApJ, 582, L15
Kormendy J., Ho L. C., 2013, ARA&A, 51, 511
Koss M., et al., 2011, ApJ, 735, L42
Koss M., Mushotzky R., Treister E., Veilleux S., Vasudevan R., Trippe M., 2012, ApJ, 746, L22
Krumpe M., Miyaji T., Husemann B., Fanidakis N., Coil A. L., Aceves H., 2015, preprint, (arXiv:1509.01261)
Liu X., Civano F., Shen Y., Green P., Greene J. E., Strauss M. A., 2013, ApJ, 762, 110
Magorrian J., et al., 1998, AJ, 115, 2285
Marconi A., Risaliti G., Gilli R., Hunt L. K., Maiolino R., Salvati M., 2004, MNRAS, 351, 169
Mazzarella J. M., et al., 2012, AJ, 144, 125
McConnell N. J., Ma C.-P., 2013, ApJ, 764, 184
McGurk R. C., Max C. E., Rosario D. J., Shields G. A., Smith K. L., Wright S. A., 2011, ApJ, 738, L2
Muldrew S. I., et al., 2012, MNRAS, 419, 2670
Müller-Sanchez F., Comerford J. M., Nevin R., Barrows R. S., Cooper M. C., Greene J. E., 2015, preprint, (arXiv:1509.04291)
Owen F. N., O'Dea C. P., Inoue M., Eilek J. A., 1985, ApJ, 294, L85
Remus R.-S., Dolag K., Bachmann L. K., Beck A. M., Burkert A., Hirschmann M., Teklu A., 2015, in Ziegler B. L., Combes F., Dannerbauer H., Verdugo M., eds, IAU Symposium Vol. 309, IAU Symposium. pp 145–148, doi:10.1017/S1743921314009491
Romanowsky A. J., Fall S. M., 2012, ApJS, 203, 17
Rosario D. J., McGurk R. C., Max C. E., Shields G. A., Smith K. L., Ammons S. M., 2011, ApJ, 739, 44
Rosas-Guevara Y. M., et al., 2015, MNRAS, 454, 1038
Schaye J., et al., 2015, MNRAS, 446, 521
Shankar F., 2013, Classical and Quantum Gravity, 30, 244001
Shankar F., Salucci P., Granato G. L., De Zotti G., Danese L., 2004, MNRAS, 354, 1020
Shankar F., Weinberg D. H., Miralda-Escudé J., 2009, ApJ, 690, 20
Shields G. A., Rosario D. J., Junkkarinen V., Chapman S. C., Bonning E. W., Chiba T., 2012, ApJ, 744, 151
Sijacki D., Springel V., Di Matteo T., Hernquist L., 2007, MNRAS, 380, 877
Sijacki D., Springel V., Haehnelt M. G., 2011, MNRAS, 414, 3656
Sijacki D., Vogelsberger M., Genel S., Springel V., Torrey P., Snyder G. F., Nelson D., Hernquist L., 2015, MNRAS, 452, 575
Springel V., 2005, MNRAS, 364, 1105
Springel V., Hernquist L., 2003, MNRAS, 339, 289
Springel V., Di Matteo T., Hernquist L., 2005, MNRAS, 361, 776
Steinborn L. K., Dolag K., Hirschmann M., Prieto M. A., Remus R.-S., 2015, MNRAS, 448, 1504
Teklu A. F., Remus R.-S., Dolag K., Beck A. M., Burkert A., Schmidt A. S., Schulze F., Steinborn L. K., 2015, ApJ, 812, 29
Tornatore L., Borgani S., Springel V., Matteucci F., Menci N., Murante G., 2003, MNRAS, 342, 1025
Tornatore L., Borgani S., Dolag K., Matteucci F., 2007, MNRAS, 382, 1050
Treister E., Schawinski K., Urry C. M., Simmons B. D., 2012, ApJ, 758, L39
Tremaine S., et al., 2002, ApJ, 574, 740
Van Wassenhove S., Volonteri M., Mayer L., Dotti M., Bellovary J., Callegari S., 2012, ApJ, 748, L7
Vogelsberger M., Genel S., Sijacki D., Torrey P., Springel V., Hernquist L., 2013, MNRAS, 436, 3031
Vogelsberger M., et al., 2014, Nature, 509, 177
Volonteri M., Madau P., 2008, ApJ, 687, L57
Volonteri M., Bogdanovic T., Dotti M., Colpi M., 2015a, preprint, (arXiv:1509.09027)
Volonteri M., Capelo P. R., Netzer H., Bellovary J., Dotti M., Governato F., 2015b, MNRAS, 449, 1470

	68Mpc/uhr	182Mpc/uhr
$z = 2.0$	$(0.5 \pm 0.2)\%$	$(1.2 \pm 0.3)\%$
$z \leqslant 0.21$	$> (2.1 \pm 0.6)\%$	–

Table 3. Fraction of dual and offset AGN with respect to the total number of AGN at $z = 2$ and $z = 0$ for two different uhr simulations: the 68Mpc/uhr simulation is described in Teklu et al. (2015) and the larger 182Mpc/uhr is used for this work. The given errors are $\sqrt{N}/N_{\rm tot}$ errors.

Wiersma R. P. C., Schaye J., Smith B. D., 2009, MNRAS, 393, 99
Yu Q., Lu Y., Mohayaee R., Colin J., 2011, ApJ, 738, 92

APPENDIX A: FRACTION OF DUAL AND OFFSET AGN AT Z=0

Since our large volume simulation only ran down to $z = 2$, we use the smaller volume of 68Mpc (Teklu et al. 2015, Remus et al. in prep.), which ran until $z = 0$, to estimate the expected fraction of AGN pairs at $z \leqslant 0.21$, which is the redshift range from Comerford & Greene (2014). The 68Mpc/uhr simulation has five snapshots in the range $z \leqslant 0.21$. Since the life time of an AGN is much shorter than the time interval between our snapshots, we can use all of these snapshots to select BH pairs. In that way, we get enough BH pairs, although one snapshot alone is too small to be statistically relevant. However, the smaller simulation has problems in reproducing a realistic mass and luminosity distribution of AGN, because it does not contain the new implementations from Steinborn et al. (2015). This can lead to differences in the fraction of dual and offset AGN, since the new model is especially sensitive in the case of mergers where AGN accrete with high Eddington ratios. Here, BHs with masses above $\sim 10^8 M_\odot$ accrete more efficiently and subsequently transit faster to the more inefficient jet-mode. In addition, the BHs in the 68Mpc/uhr simulation need longer to grow above the resolution limit of $10^7 M_\odot$. Consequently, more BHs lie right below this limit. This is visible when comparing the BH mass functions shown in Hirschmann et al. (2014) and Steinborn et al. (2015) with each other. For that reason a direct comparison of the fraction of dual and offset AGN in the two simulations would not be very meaningful but still, the overall spatial distribution of the BHs and AGN is very valuable also in the 68Mpc/uhr simulation, mainly because we do not pin the BHs artificially to the most bound particle.

Hence, we consider all BHs and all dual and offset AGN in the 68Mpc/uhr simulation at $z = 2.0$ and $z < 0.21$, also the unresolved ones, and subsequently, we assume that the same fraction as in the 182Mpc/uhr simulation is resolved. For all BHs these are 92.51% and for dual and offset AGN it are 82.14%. With this assumption, we find a fraction of $\sim 0.5\%$ at $z = 2.0$. For $z < 0.21$ we expect that $\sim 2.1\%$ of all AGN are dual or offset AGN (Table 3), which is clearly higher than the observed values mentioned above (Rosario et al. 2011, Fu et al. 2011a, Comerford & Greene 2014). Possible reasons for this large value might be our limited mass resolution due to which we consider only BHs with $M_\bullet < 10^7 M_\odot$ and our chosen luminosity threshold for AGN.

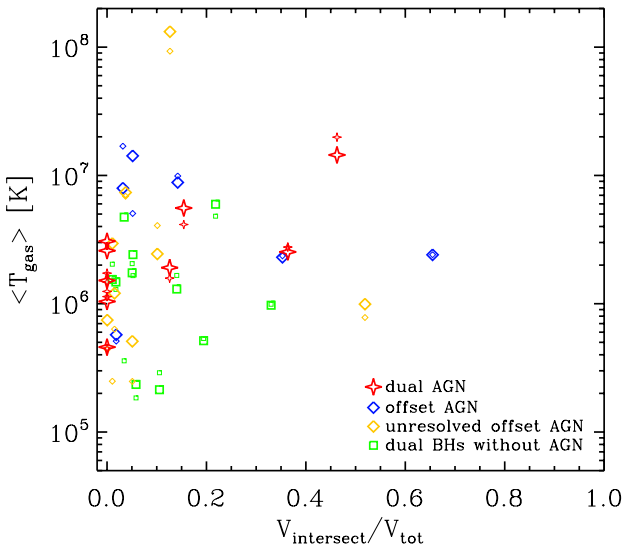

Figure 15. Fraction of the intersection of the volumes used to calculate the accretion rate with respect to the total volume compared with the mean gas temperature inside the accretion radius of each BH.

Furthermore, we do not consider obscuration in this work. We suspect that the fraction of dual and offset AGN is larger at low redshifts, since more AGN are triggered by mergers in contrast to smooth gas accretion. However, our prediction for $z < 0.21$ is rather uncertain, because we assume that the same fraction of BHs is not resolved like at $z = 2.0$, but since the BHs are in general more massive at lower redshifts the fraction of resolved BHs should be larger. If this affects dual and offset AGN in the same way, this effect would cancel out, but since AGN are in general more massive BHs, our prediction can only be seen as a lower limit.

APPENDIX B: INTERSECTION BETWEEN ACCRETION RADII

Fig. 15 and 16 demonstrate that our analysis is not diven by numerical effects due to our BH model. $V_{\rm intersect}$ is the volume inside the accretion radius which intersects between the two BHs and $V_{\rm tot} = V_1 + V_2 - V_{\rm intersect}$ is the total volume. Since both dual and offset AGN spread over the whole range of $V_{\rm intersect}/V_{\rm tot}$ we can exclude that the two different classes are a numerical effect due to our choice of the accretion radius. There is one trend visible, namely that most dual AGN do not intersect at all and as soon as they intersect we have much more offset AGN than dual AGN. Many pairs without AGN have a very low gas temperature, because the BH has just been seeded and the galaxy is not very evolved yet. Of course this can be an effect of the seeding model. The few offset AGN with high gas temperatures seem indeed to be triggered by AGN feedback, whereas for the others feedback does not play an important role. The BH masses of the one dual AGN with an extremely high gas temperature are very similar such that none of the two BHs dominates over the other one.

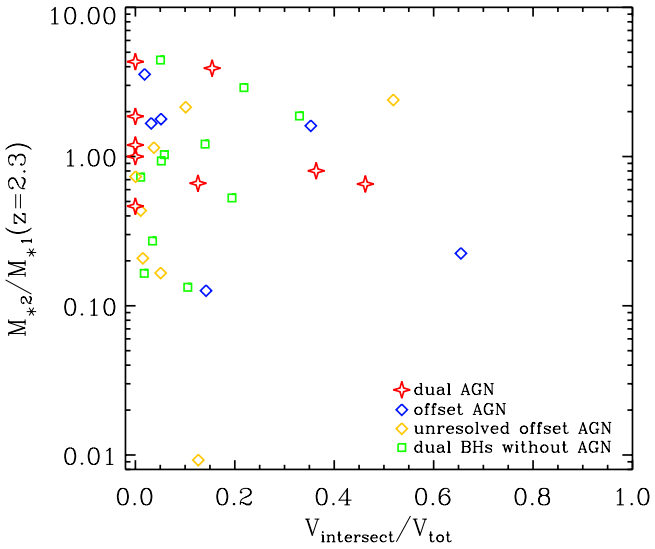

Figure 16. Fraction of the intersection of the volumes used to calculate the accretion rate with respect to the total volume compared with the stellar mass ratio, where M_{*1} and M_{*2} correspond to the more and less luminous BH at $z = 2.0$, respectively.

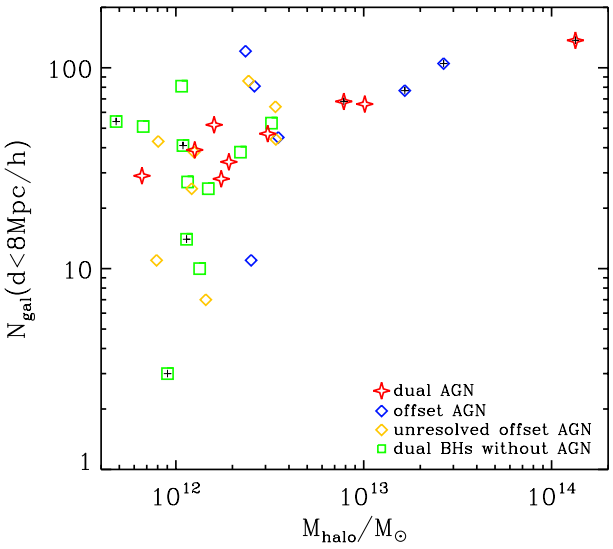

Figure 18. Number of neighbour galaxies within a radius of 8Mpc/h which are larger than $10^{10} M_\odot$. The black crosses mark mergers between two substructures, i.e. they do not occur in the central galaxy.

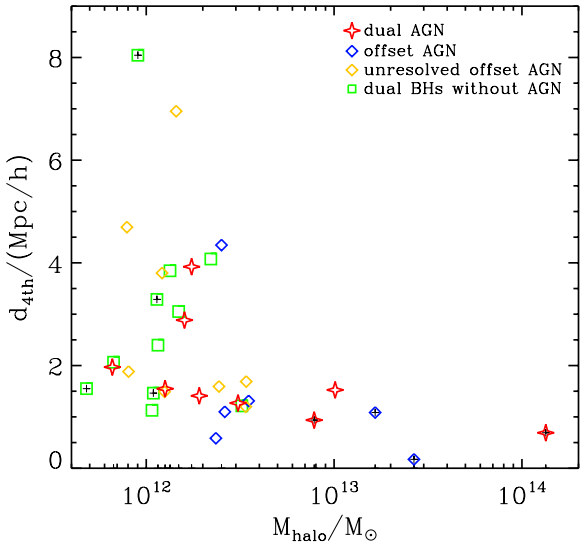

Figure 17. Distance to the forth nearest neighbour galaxy with $M_* > 10^{10} M_\odot$. The black crosses mark mergers between two substructures, i.e., they do not occur in the central galaxy.

APPENDIX C: ENVIRONMENT

In Fig. 17 and Fig. 18 we show two different measures of the environment against the total the dark matter halo: i) the distance to the 4th nearest galaxy and ii) the number of galaxies within a radius[6] of 8Mpc/h (e.g. Haas et al. 2012, Muldrew et al. 2012 and references therein). For both approaches we choose a mass threshold of $M_* > 10^{10} M_\odot$ for the neighbouring galaxies (Baldry et al. 2006). Especially in Fig. 18 it is visible that both dual and offset AGN prefer a dense environment, although BH pairs without AGN can as well have many neighbouring galaxies. The two figures also show that all simulated BH pairs in haloes with $M_{\rm halo} > 4 \cdot 10^{12} M_\odot$ contain at least one AGN. Hence, looking for a dense environment might help to find dual and offset AGN, although we also produce them in less denser environments.

Furthermore, the two figures show clearly that our simulation produces offset AGN only in haloes above $M_{\rm halo} \approx 2 \cdot 10^{12} M_\odot$. Below that threshold there are only unresolved offset AGN. In contrast, dual AGN scatter over the whole range of halo masses. This might be a consequence of our findings that dual AGN are often in major mergers, whereas differences in the BH and stellar mass can cause offset AGN, because offset AGN in low mass haloes need, in contrast to dual AGN, an even less massive counterpart and hence the smaller BH mass is not resolved. Considering this resolution effect, we do not see a different environment of dual and offset AGN. However, the approaches used to measure the environment are both spherically symmetric and thus, large-scale filaments are not captured by this method. Hence, it turned out that measuring the gas accretion history like in Fig. 12 is more useful to investigate AGN triggering mechanisms.

In Fig. 17 and Fig. 18 we also mark mergers between two substructures with black crosses, in contrast to mergers involving the central galaxy. Although our sample contain only a few groups and only one cluster at $z = 2.0$, it is a remarkable result that most of the mergers in these massive haloes occur between two substructures. This might indicate that, at least at such a high redshift, the central galaxy does not yet play such a dominant role as known from the local universe.

[6] We tested several radii and it turned out that using 8 Mpc/h it is best visible that both dual AGN prefer a denser environment.

This paper has been typeset from a TEX/LATEX file prepared by the author.